

Multiwavelength lidar aerosol measurements made at Eureka (80°N,86°W) during early 1995

D.P. Donovan^{1,2}, A.I. Carswell¹, T. Shibata³, J.C. Bird¹, T.J. Duck¹, T. Itabe⁴, T. Nagai⁵, S.R. Pal¹, O. Uchino⁶, and J.A. Whiteway^{1,7}

Abstract. Principal Component Analysis (PCA) aerosol retrievals have been applied to multiwavelength lidar measurements made in early 1995 in the Canadian Arctic. The lidar data have been inverted to provide estimates of stratospheric aerosol volume, surface area, effective radius, and sulfate mass mixing ratio. Above the vortex lower boundary the aerosol parameters were relatively constant but changed notably in the sub-vortex region throughout the winter.

Introduction

Aerosols play a number of important roles in the winter polar stratosphere. In particular, they play a key role in polar ozone chemistry. At temperatures below about 195 K, the background liquid mainly sulfate/water aerosols can participate in the heterogeneous chemical conversion of chlorine from inactive to active forms [Del Negro *et al.*, 1997]. At temperatures below about 193 K, they may grow significantly via absorption of HNO₃ and water [Carslaw *et al.*, 1995] leading to polar stratospheric cloud (PSC) formation. Stratospheric aerosols can also serve as tracers of air motion.

To study the role of stratospheric aerosols quantitative measurements of the aerosol physical properties are necessary. In general, reliable detailed size distribution information can not be extracted from a few backscatter and/or extinction measurements [Müller and Quenzel, 1984]. However, it is possible to make reliable estimates of quantities related to the lower moments of the size distribution such as surface area and volume density.

In this paper Principal Component Analysis (PCA) is applied to a long time series of multiwavelength lidar measurements. The lidar measurements were made during January to March of 1995 at the Eureka NDSC (Network for Detection of Stratospheric Change) observatory in the Canadian high Arctic.

Principal Component Analysis

PCA as applied in this work has been extensively described elsewhere [Donovan and Carswell, 1997] (hereafter referred to as P1) so only a brief overview will be given here.

¹Center for Research in Earth and Space Technology, York U. Dept. of Physics and Astronomy, North York, ON., Canada.

²Now at: Royal Netherlands Meteorological Institute (KNMI), De Bilt, the Netherlands.

³Solar-Terrestrial Environmental Laboratory (STEL) Nagoya University, Nagoya, Japan.

⁴Communications Research Laboratory (CRL) Tokyo, Japan.

⁵Meteorological Research Institute (MRI) Tsukuba, Japan.

⁶Japan Meteorological Agency (JMA), Japan.

⁷Now at: Dept. of Physics, University of Wales, Aberystwyth, Ceredigion, UK.

Copyright 1998 by the American Geophysical Union.

Paper number 98GL52328.
0094-8534/98/98GL-52328\$05.00

In matrix form, the relationship between a set of optical measurements and the unknown aerosol size distribution can be written as,

$$\bar{\mathbf{g}} = \mathbf{K}\bar{\mathbf{v}} + \bar{\mathbf{e}} \quad (1)$$

where $\bar{\mathbf{g}}$ is the measurement vector, $\bar{\mathbf{v}}$ is the size distribution vector, $\bar{\mathbf{e}}$ is the measurement error vector and \mathbf{K} is the kernel matrix constructed using discrete forms of the appropriate backscatter and/or extinction efficiencies. A PCA retrieval may then be used to invert Eqn. 1 to recover an estimate of $\bar{\mathbf{v}}$.

The details of the recovered size distribution may not be reliable. However, estimates of the quantities related to the lower moments of the size distribution do tend to be reliable. The PCA estimate of any given integral quantity of the size distribution (P) can be expressed as [Thomason and Poole, 1993]

$$P = \bar{\mathbf{a}}^t \bar{\mathbf{g}} \quad (2)$$

where $\bar{\mathbf{a}}^t$ is a vector of the appropriate PCA coefficients. Thus, the estimated value of any integral parameter can be expressed as a linear combination of the measurements without evaluating the size distribution.

The statistical uncertainty of a given PCA approximation is influenced by the number of *principal component functions* retained in deriving the coefficients. To reduce the statistical uncertainty of the PCA estimates in this work, only the two lowest order component functions are retained for aerosol surface area while the three lowest order components are retained for estimating the aerosol volume [P1].

Lidar Measurements

Two lidars are located at Eureka. The AES/CRESTech Raman DIAL system uses a 65 Watt XeCl laser and a 1 meter diameter telescope [Pal *et al.*, 1996] and is used to make measurements of the aerosol backscatter and extinction using the elastic and Raman 'off' wavelength pair (353/385nm). For detection, the DIAL uses photon-counting (PC) photomultiplier tubes (PMTs) together with a mechanical chopper and neutral density (ND) filters to insure the linearity of the detected returns [Donovan *et al.*, 1993]. The MRI/CRL Nd:YAG system is used to make aerosol backscatter and depolarization measurements. It transmits 4 Watts at both 1064 and 532 nm and uses a 0.5 meter receiver for the IR channel and a 0.25 meter telescope for the green channel [Nagai *et al.*, 1997]. This system also uses PC PMTs and variable ND filters.

Figure 1 shows a typical example of a set of backscatter ratio ($R=1.0 + \beta_{\pi,aerosol}/\beta_{\pi,molecular}$) and extinction measurements. The observations shown here are an average of the night's data (typically several hours). The backscatter profiles were normalised to 1 at altitudes above the aerosol layer. Aerosol extinction effects in the backscatter retrievals were accounted for by using PCA relationships to predict the aerosol extinction. The temperature and density profiles used were deduced from radiosondes launched at least twice

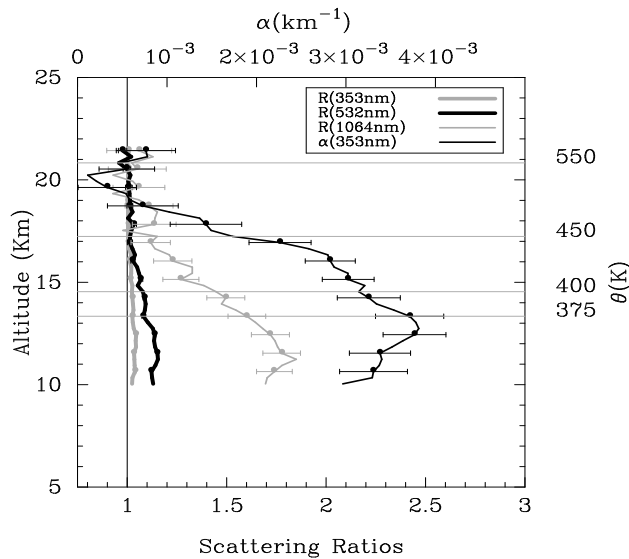


Figure 1. Lidar scattering ratios and 353nm aerosol extinction measured over Eureka February 21, 1995. The grey horizontal lines show the potential temperature (θ) for 4 different geometric altitudes.

daily. To deduce the aerosol refractive index a constant water vapor mixing ratio of 5 ppm was assumed [Russell and Hamill, 1984]. The variation of the aerosol refractive index due to possible HNO_3 uptake was not considered.

Figure 2 shows the volume density (V), surface area density (SA), and the effective radius ($3V/SA$) predicted using the data shown in Figure 1. The error bars denote the statistical error limits ($\pm 1\sigma$) while simulations indicate that the estimates are likely accurate to within 20% for the surface area and volume and within 30% for the effective radius [P1]. The effective radii shown here are consistent with those previously measured at mid and high latitudes while the surface area and volume densities are lower than those measured in the Arctic during winter 92/93 ($V \approx 1.6 \mu\text{m}^3/\text{cm}^3$ at 400 K [Beyerle et al., 1997]) and winter 93/94 ($V \approx 1.0 \mu\text{m}^2/\text{cm}^3$, $SA \approx 15 \mu\text{m}^2/\text{cm}^3$ at 400 K [P1]) but still higher than

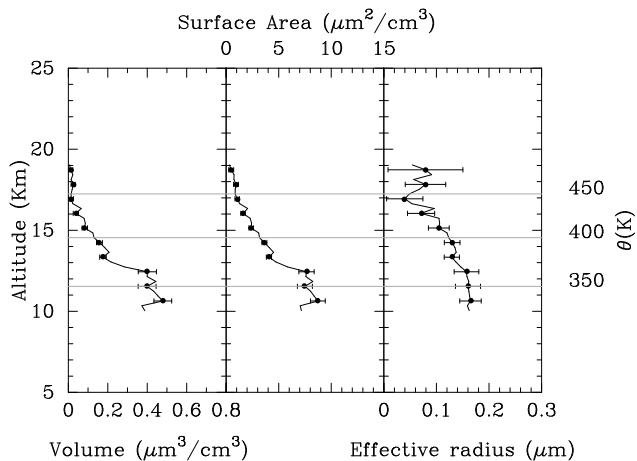


Figure 2. Aerosol volume, surface area, and effective radius for the data shown in Figure 1.

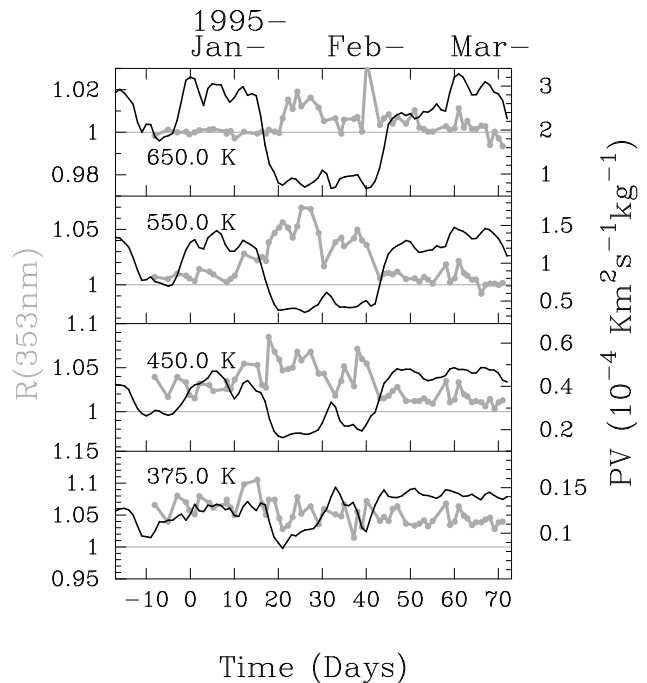


Figure 3. Scattering ratio at 353 nm (grey) and NMC potential vorticity (dark line) over Eureka. The data shown have been averaged ± 25 K around the indicated θ value.

those measured during pre-Pinatubo conditions in 89/90 ($SA \approx 2.5 \mu\text{m}^2/\text{cm}^3$ at 400 K [Wilson et al., 1992]).

Observations

During the winter of 1994/95 the stratosphere over Eureka was, on occasion, both clearly inside and outside of the polar vortex. Figure 3 shows a time series of the observed scattering ratio at 353 nm along with the potential vorticity given by the NMC objective analysis. Above 450 K it can be seen that periods inside of the vortex (high PV) correspond to lower R values.

Figure 4 shows the average scattering ratio profiles for 353 and 1064 nm for four selected time periods as a function of potential temperature. From Jan. 1-16 (period 1) Eureka was inside the polar vortex. From Jan. 20 to Feb. 7 (period 2) the stratosphere above Eureka was clearly outside the vortex, while from February 14 onwards (periods 3 and 4) Eureka was clearly inside of the vortex. The error bars give the standard deviation of the mean profile. Only cases where no strong depolarization signatures (indicating the presence of non-spherical particles) were present were used here. Non-spherical PSC scatterers were found to be present over Eureka in mid-December 1994 and early January 1995 [Nagai et al., 1997]. After censoring the data with regard to the presence of non-spherical particles, the temperatures then considered were generally well above those where significant HNO_3 uptake would be expected [Carshaw et al., 1995].

Two main points can be made regarding Figure 4. First, as expected, the scattering ratios above the vortex lower boundary (about 410 K) at both wavelengths were greatly enhanced during period 2. This reflects the fact that transport across the vortex boundary is small and that the aerosol

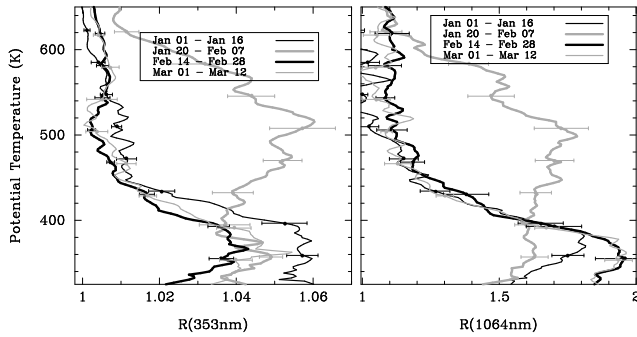


Figure 4. Average scattering ratio profiles at 353 and 1064 nm for 4 selected periods.

concentration inside the vortex is very low compared to mid-latitude stratospheric air at altitudes above about 410 K. The second point can be seen by considering the scattering ratio profiles below 400 K. Here, the scattering ratios at 353 nm and 532 nm (not shown) decrease with time, while at 1064 nm a notable increase between period 1 and periods 3 and 4 is evident. This indicates that the aerosol size distribution in March must have been notably different from that in January.

Given the different scattering ratio trends at different wavelengths deducing reliable aerosol information using single wavelength observations would be problematic. However, using PCA we can examine the derived aerosol physical parameter trends. The average retrieved aerosol physical characteristics corresponding to Figure 4 are presented in Figure 5. The trends in Figure 5 are more consistent than those that may be expected from looking at Figure 4. In particular, below 400 K, the aerosol physical parameters decrease with time regardless of the fact that the scattering ratios at 1064 nm were seen to increase with time. This point will be discussed further later on.

To account for the observed changes in the aerosol optical and physical properties the occurrence of diabatic descent must be first taken into account. Since particle adjustment due to changes in ambient water vapor concentration happens on short time scales (hours to days) sulfate mixing ratio is more likely to act as a conserved tracer over the other calculated quantities [Thomason and Poole, 1993]. Assuming

that the sulfate mixing ratio is conserved leads to a mean diabatic descent rate of about 0.45 K/day between early January and early March in the 440–400 K range. This descent rate is in line with other estimates [Rosenfield *et al.*, 1994].

Allowing for diabatic descent removes much of the observed temporal variation in the inside vortex aerosol parameters around the 400–440 K levels shown in Figure 5. However, considerable variation still exists in the sub-vortex region (below 400 K). Here sulfate mixing ratios decrease from values around 2.2 ppbm for period 1 to values around 1.6 ppbm for period 4. Periods 1 and 2 share similar sulfate mixing ratios. However, period 1 has notably larger volume and surface area mixing ratios. This may be explained by considering that period 2 was considerably warmer than period 1. Period 2 had a mean temperature of 225 K giving an average aerosol sulfate weight percentage of around 72% versus 60% for period 1 ($T=205$ K). This would be expected to produce a decrease in volume of around 30% [Carslaw *et al.*, 1995] which is in line with the observed reduction in volume mixing ratio between periods 1 and 2.

By accounting for diabatic descent and using the estimates of aerosol volume and effective radius we can account for the apparently contradictory scattering ratio trends below 400 K at the different measurement wavelengths. It happens that the aerosol volume backscattering efficiency at 1064 nm and the volume extinction efficiency at 353 nm both possess broad peaks around $0.2 \mu\text{m}$ while the volume backscatter efficiencies at 353 and 532 nm possess local minima close to $0.2 \mu\text{m}$ (see [P1]). Thus, for a given size distribution, increasing the number of particles around $0.2 \mu\text{m}$ will increase the relative backscattering and extinction at 1064 nm and 353 nm respectively while decreasing the volume normalised backscattering at 532 and 353 nm. This is illustrated in Figure 6 which shows the backscattering and aerosol extinction per unit aerosol volume as a function of R_{eff} for two single mode lognormal distributions with mode widths (σ_w) of 1.3 and 1.8. The distributions have been scaled so that their total volume matches our results. Figure 6 also shows the appropriate observed values at 375 K after accounting for diabatic descent for periods 1 and 3. The results using the lognormal distributions are broadly consistent with the PCA results. Here the increase in the volume scattering efficiency at 1064 nm is enough to produce the observed increase in scattering even though the

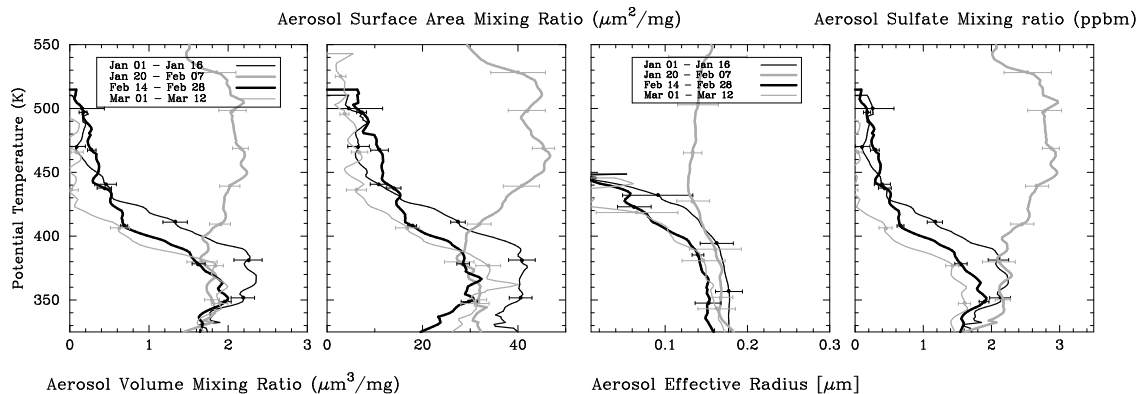


Figure 5. Estimated aerosol volume density, surface area, effective radius, and sulfate mass mixing ratio for the data shown in Figure 4.

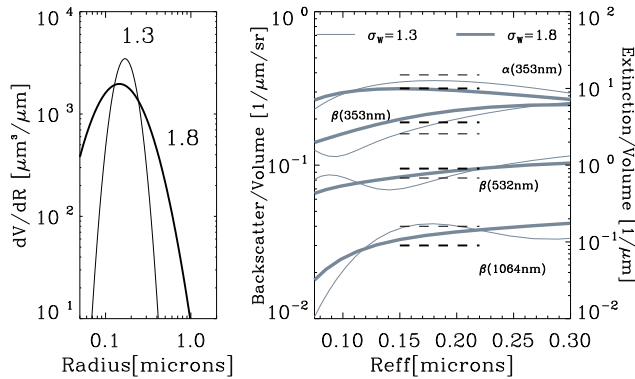


Figure 6. Two lognormal distributions, both with $R_{eff} = 0.18\mu\text{m}$ but with different mode widths (left) and the backscatter and extinction per unit aerosol volume as a function of effective radius for distributions of both widths (right). The thick dashed lines denote the observed scattering values for the January 1-8 time period while the thin dashed lines give the values observed during February 14 - March 12.

total aerosol volume has decreased. The results here are mainly qualitative in nature, the key point is that relative to period 1, periods 3 and 4 appear to have had relatively more particles with radii around 0.15-0.2 microns present.

Summary

Because of the low amount of aerosol above within the polar vortex above 450 K the Eureka data are most useful for studying the morphology of the stratospheric aerosol in the lowermost vortex and sub-vortex regions. Our results indicate that in the 400 to 410 K region the vortex aerosol properties over Eureka were relatively constant throughout the winter. In the sub-vortex region however, sulfate amounts decreased throughout the winter and the aerosol size distribution was seen to notably change. In particular, relative to the early winter the late winter sub-vortex aerosol layer appeared to have more particles with radii around 0.15-0.2 microns present in spite of the general decrease in total aerosol amounts. However, the significance of this result is unclear due to the uncertain source of the sampled air. Unlike the vortex, the sub-vortex is not generally isolated from mid-latitudes, this implies that it is problematic to attribute the observed early and late winter difference in the aerosol in this region as being due to specific physical processes (i.e.

sedimentation, growth) and not being due to differences in transport.

Acknowledgments. Financial and technical support was provided by CRESTech and by the Canadian AES. The financial support of NSERC and the Japanese STA is also gratefully acknowledged.

References

- Beyerle, G. et al., Temperature dependence of ternary solution particle volumes as observed by lidar in the Arctic stratosphere during winter 1992/93, *J. Geophys. Res.*, *103*, 3604-3608, 1997.
- Carlsaw, K.S., B. Lou and T. Peter, An analytical expression for the composition of aqueous $\text{HNO}_3\text{-H}_2\text{SO}_4$ stratospheric aerosols including gas phase removal of HNO_3 gas phase depletion from coupled HNO_3 and water uptake by liquid particles, *Geophys. Res. Letts.*, *22*, 1877-1880, 1995.
- Donovan D.P. and A.I. Carswell, Principal component analysis applied to multiwavelength lidar aerosol backscatter and extinction measurements, *Appl. Opt.*, *36*, 9406-9424, 1997.
- Donovan D.P. J.A. Whiteway, and A.I. Carswell, Correction for nonlinear photon-counting effects in lidar systems, *Appl. Opt.*, *32*, 6742-6753, 1993.
- Del Negro L.A. et al., Evaluating the role of NAT, NAD, and liquid $\text{H}_2\text{SO}_4/\text{H}_2\text{O}/\text{HNO}_3$ solutions in Antarctic polar stratospheric cloud aerosol: Observations and implications, *J. Geophys. Res.*, *102*, 13225-13282, 1997.
- Müller H. and H. Quenzel, Information content of multispectral lidar measurements with respect to the aerosol size distribution, *Appl. Opt.*, *24*, 648-654, 1984.
- Nagai T. et al., Polar stratospheric clouds observed at Eureka (80°N , 86°W) in the Canadian Arctic during the 1994/95 winter, *Geophys. Res. Letts.*, *24*, 2243-2246, 1997.
- Pal S.R. et al., Lidar Measurements of the Stratosphere at the Eureka and Toronto NDSC Stations, *SPIE*, *2833*, 28-39, 1996.
- Rosenfield J.E., P.A. Newman, and M.R. Schoeberl, Computations of diabatic descent in the stratospheric polar vortex, *J. Geophys. Res.*, *99*, 16677-16689, 1994.
- Russell P.B. and P. Hamill, Spatial variation of stratospheric aerosol acidity and model refractive index: Implications of recent results, *J. Atmos. Sci.*, *41*, 1781-1790, 1984.
- Thomason L.W. and L.R. Poole, Use of Stratospheric Aerosol Properties as Diagnostics of Antarctic Vortex Processes, *J. Geophys. Res.*, *98*, 23003-23012, 1993.
- Wilson J.C. et al., Stratospheric Sulfate Aerosol in and Near the Northern Hemisphere Polar Vortex, *J. Geophys. Res.*, *97*, 7997-8013, 1992.

D.P. Donovan, Royal Netherlands Meteorological Institute (KNMI) P.O. box 201, 3730 AE De Bilt, the Netherlands (e-mail: donovan@knmi.nl)

(Received April 21, 1998; revised June 26, 1998; accepted July 9, 1998.)